

Dipole force free optical control and cooling of nanofiber trapped atoms

C. Østfeldt, J.-B. Béguin, F. T. Pedersen, E. S. Polzik, J. H. Müller,* and J. Appel*
 QUANTOP, Niels Bohr Institute, University of Copenhagen, Blegdamsvej 17, 2100 Copenhagen, Denmark
 (Dated: February 1, 2022)

The evanescent field surrounding nano-scale optical waveguides offers an efficient interface between light and mesoscopic ensembles of neutral atoms. However, the thermal motion of trapped atoms, combined with the strong radial gradients of the guided light, leads to a time-modulated coupling between atoms and the light mode, thus giving rise to additional noise and motional dephasing of collective states. Here, we present a dipole force free scheme for coupling of the radial motional states, utilizing the strong intensity gradient of the guided mode and demonstrate all-optical coupling of the cesium hyperfine ground states and motional sideband transitions. We utilize this to prolong the trap lifetime of an atomic ensemble by Raman sideband cooling of the radial motion, which has not been demonstrated in nano-optical structures previously. Our work points towards full and independent control of internal and external atomic degrees of freedom using guided light modes only.

PACS numbers: 42.50.Ct, 37.10.De

Keywords: Quantum Optics, Cooling, Nanofiber, Nanooptics

Light guided by nanooptical waveguide- and resonator structures propagates partly as an evanescent wave; its tight sub-wavelength confinement allows for strong interactions between guided light and single atoms [1–4] or atomic ensembles [5–11] trapped within the confined field.

The inherent intensity gradients of evanescent modes are a necessity for the realization of dipole traps close to the surface of the structure. However, if the atoms are probed or manipulated also by evanescent modes, the gradients lead to detrimental effects, such as time-dependent coupling for moving atoms, additional quantum partition noise in probing atomic ensembles and motional dephasing of collective internal quantum states. As strong gradients imply strong dipole forces for any Stark shift induced by guided light, a scheme for optical manipulation of the internal degrees of freedom without perturbation of the motional state is desirable.

Additionally, any non-zero temperature above the motional quantum ground state potentially decreases the average interaction of atoms with the guided light mode, reducing the single atom optical depth (OD).

Previous results for addressing these challenges in the nanofiber platform [12] include microwave cooling of the azimuthal degree of freedom [13] by exploiting the state-dependency of the trapping potentials for different Zeeman sub-states, as well as polarization gradient cooling [6].

In this paper, we present a Raman coupling scheme that allows us to drive coherent transfers on the hyperfine transition in cesium (Cs) as well as radial motional sideband transitions, while canceling all quadratic ac-Stark shifts and thus dipole forces. Driving Raman transitions

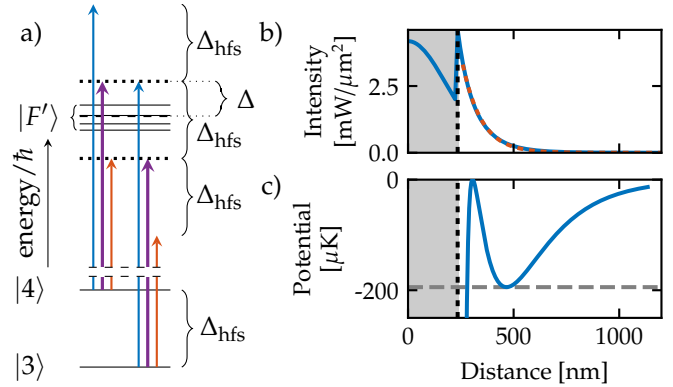


Figure 1. a) Stark shift canceling Raman scheme. The hyperfine ground states are coupled through two virtual levels (dotted lines) located symmetrically around the excited state manifold. The coupling fields are created by phase-modulation of a carrier field. By choosing the carrier detuning, $\Delta \approx \Delta_{\text{hfs}}/2$ and the ratio of the sideband to carrier powers $A = (J_1(z)/J_0(z))^2 \approx 1.5$, the ac-Stark shifts are canceled. A π phaseshift of the red-detuned sideband compared to the blue-detuned sideband ensures constructive interference of the Raman coupling amplitudes. b) Intensity of 1 mW of light ($\lambda = 852$ nm) guided by a nanofiber ($\varnothing = 470$ nm) as a function of distance to the fiber axis, together with an exponential fit (dotted line). c) Trapping potential for Cs atoms in the electronic ground state. See main text for details.

with a single beam propagating through the waveguide, we implement a cooling protocol that relies on the gradient of the coupling strength rather than its phase [14].

A key ingredient in our experimental implementation is the Stark shift canceling Raman coupling scheme presented in Fig. 1a: We couple the hyperfine ground states $|F = 3\rangle$ and $|F = 4\rangle$ via two simultaneous two-photon Raman processes. This is achieved by phase modulation (PM) of a single optical field with a modulation frequency $\omega_{\text{sb}} = \Delta_{\text{hfs}} + \delta$, close to the hyperfine ground state split-

* Corresponding Authors: jappel@nbi.dk; muller@nbi.dk

ting Δ_{hfs} . The carrier field is detuned $\Delta \sim \Delta_{\text{hfs}}/2$ above the transition from $|6^2S_{1/2}, F=4\rangle$ to the $|6^2P_{3/2}, F'\rangle$ manifold. By choice of the absolute frequencies and powers of the fields, we cancel the quadratic ac-Stark shifts.

To present the basic idea, we assume an initial field $E(t) = E_0 e^{i\omega t}$ subject to pure PM and neglect sidebands of order two and higher

$$E(t) = E_0 J_0(z) e^{i\omega t} \left[1 + \sqrt{A} \left(e^{+i\omega_{\text{sb}} t} - e^{-i\omega_{\text{sb}} t} \right) \right], \quad (1)$$

where A denotes the ratio of sideband-to-carrier power $A = (J_1(z)/J_0(z))^2$, z is the phase modulation index, ω_{sb} is the modulation frequency, and J_n is the n^{th} Bessel function of the first kind.

Neglecting hyperfine splitting of the upper state manifold, which is much smaller than the single photon detuning Δ , one obtains simultaneous cancellation of the quadratic ac-Stark shifts for both lower levels with $A = 1.5$ and $\Delta = \Delta_{\text{hfs}}/2$. A more complete numerical analysis of the parameter landscape including higher order PM-sidebands and the excited state hyperfine splitting confirms that Δ predominantly determines the common mode light shift, while A controls the differential light shift.

As the two (dominating) Raman couplings will add coherently, their phase must be taken into account. Specifically, the transition through the lower virtual level will acquire a minus-sign with respect to the upper transition from the fact that the single-photon detuning is opposite. Constructive interference of the Raman coupling amplitudes is ensured by the π -phase shift of the lower sideband relative to the carrier and upper sideband inherent to PM – see (1).

The experimental setup is explained in detail elsewhere [7], the salient features are summarized as follows. A standard step-index fiber (Thorlabs 780HP) is tapered down to sub-wavelength diameter ($d = 470$ nm), so that light propagating in the nanofiber is guided partly as an evanescent wave. We create a dipole trap consisting of two quasi-linearly co-polarized counter-propagating red-detuned beams ($\lambda = 1056$ nm, $P = 2 \times 1.6$ mW) and one blue-detuned running wave field ($\lambda = 780$ nm, $P = 8.5$ mW) in the orthogonal quasi-linear polarization [5]. The resulting trap potential, evaluated at the axial minimum, is shown in Fig. 1c. Axially, two strings of potential wells are located on opposite sides of the fiber, allowing us to trap ~ 2000 atoms. Atoms are loaded into the trap by a standard 6-beam magneto-optical trap (MOT) setup, followed by sub-Doppler cooling [5, 7].

We detect atoms in $|F=4\rangle$ using a dipole-force free dual-color heterodyne dispersive measurement scheme previously described in [7]. Atoms in $|F=3\rangle$ can be detected by transfer into the $|F=4\rangle$ -manifold and subsequent measurement there. We thus detect the optical phase shift induced by atoms in each state onto our probe light and express the data in radians.

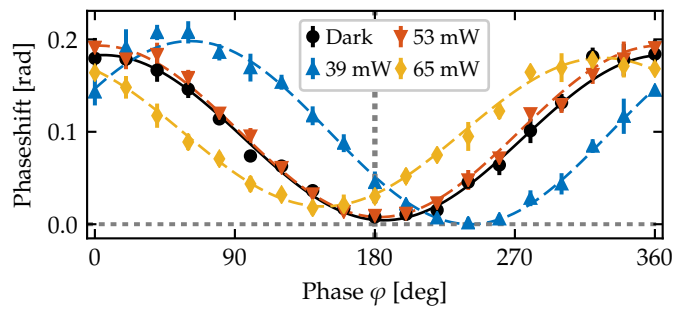


Figure 2. Ramsey fringes for varied sideband powers. An off-resonant Raman pulse perturbs the energy-splitting, leading to a shift of the fringe, φ_0 . Black solid line: Ramsey fringe in the absence of the Raman pulse. Colored dashed lines: Fringes for varied EOM drive powers. For details see main text.

The Raman light is supplied from a standard extended cavity diode laser, beatnote-locked to our MOT repump laser [15]. This leads to a flexible choice of carrier detuning, typically 4.5 GHz above the center of the transition from $|F=4\rangle$ to the $|F'=2\dots 5\rangle$ manifold.

The laser is modulated with by a EOSpace PM-0K5-10-PFA-PFA-850 fiber-coupled electro-optical modulator (EOM), driven by a RF signal derived from a AD9910 DDS, which is mixed with a stable 9 GHz frequency [16]. We measure the RF power at the EOM, which is proportional to the squared modulation index z^2 .

The Raman light is coupled as a single (co-propagating) beam into the fiber and is polarized parallel to the red trap light.

To set the phase modulation amplitude, we measure the differential shift caused by the Raman laser in a Ramsey experiment in the following way, see Fig. 2: Starting with all atoms in $|F=3, m_F=0\rangle$, the atoms are prepared in an equal superposition $(|F=3, m_F=0\rangle + |F=4, m_F=0\rangle)/\sqrt{2}$ by a microwave $\pi/2$ -pulse. We then apply a 20 μs pulse of 4.3 nW Raman light, where the PM phase is flipped by 180° every 4 ns to avoid population transfer. A second microwave $\pi/2$ -pulse with phase φ completes the Ramsey sequence, and the population in $|F=4, m_F=0\rangle$ is measured. Any differential light shift induced by the Raman light results in a shifted Ramsey fringe. By adjusting the sideband power ratios, we thus obtain cancellation of the differential shift.

We verify that for the correct single photon detuning the Raman light imposes no common mode ac-Stark shift, as we detect no modulation of our probe signal for a Raman beam with approximately 1 order of magnitude more power than used for normal coherent operations [17].

Coupling of motional states normally requires transfer of photon momentum along the important direction, or alternatively state-dependent potentials. For co-

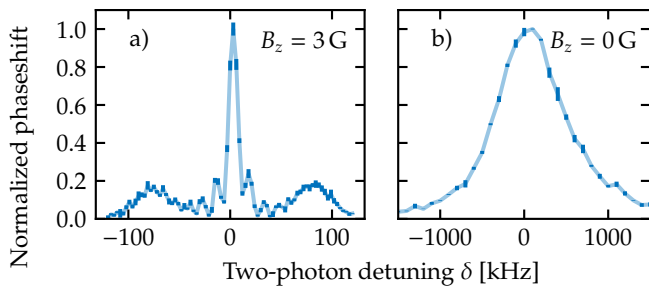


Figure 3. Typical Raman transfer spectra as a function of two-photon detuning. a) Transfer spectrum with 3 G bias field. 80 μ s pulse duration, leading to 12.5 kHz oscillatory features seen close to the central peaks. b) Transfer spectrum without magnetic bias field. All values are normalized by the maximum value. Notice the different x -axes.

propagating Raman beams like in our setup, the momentum transfer is only proportional to the wave-number difference, and in our case it vanishes along the radial direction. Instead, our scheme relies on the fast radial decay of the guided Raman light, see Fig. 1b, for coupling the radial motional states $|n\rangle$:

$$\begin{aligned} \Omega_{n,m'} &= \Omega_0 \left\langle n \left| \frac{I(\hat{\mathbf{r}})}{I(0)} \right| n' \right\rangle \\ &\approx \Omega_0 \langle n | \exp(-\hat{\mathbf{r}}/\ell) | n' \rangle, \end{aligned} \quad (2)$$

where $I(\hat{\mathbf{r}})$ is the intensity at position $\hat{\mathbf{r}}$, ℓ is the radial decay length of the intensity, Ω_0 is the Raman Rabi frequency for an atom located at the trap minimum $\hat{\mathbf{r}} = 0$, and $\hat{\mathbf{r}}$ is the position-operator in the radial direction [18]. In analogy to the phase gradient of a plane wave $\exp(i\mathbf{k}\mathbf{r})$, the radial decay acts effectively as “imaginary momentum”. The coupling scales with the ratio of the motional wavefunction size \tilde{r} to ℓ . This quantity plays the role of the Lamb-Dicke parameter [19], and inserting for \tilde{r} the ground state wave packet size we obtain $\tilde{r}/\ell \approx 1/5$.

To investigate the Raman transfer efficiency, we prepare atoms in the state $|F=3, m_F=0\rangle$, and transfer them into $|F=4, m_F=0\rangle$ using a resonant two-photon Raman pulse. In Fig. 3 we show the transfer spectrum with and without a 3 G magnetic bias field, aligned parallel to the polarization of the blue-detuned trap field.

In Fig. 3a we observe for $\delta \equiv \omega_{\text{sb}} - \Delta_{\text{hfs}} \sim 0$ Hz a motional carrier transition, i.e. a transition that changes only the internal state of the atom. For $\delta \sim \pm(60 \text{ kHz} - 125 \text{ kHz})$ we clearly resolve the motional sidebands, demonstrating that we can couple the motional states coherently. The sideband splitting is consistent with the calculated frequency of the radial motion, and the width of the sidebands stems from the spread of vibrational frequencies, due to the anharmonic shape of the trap, see Fig. 1c.

In Fig. 3b we plot a typical transfer spectrum without the usual magnetic bias field. By removal of this field, the

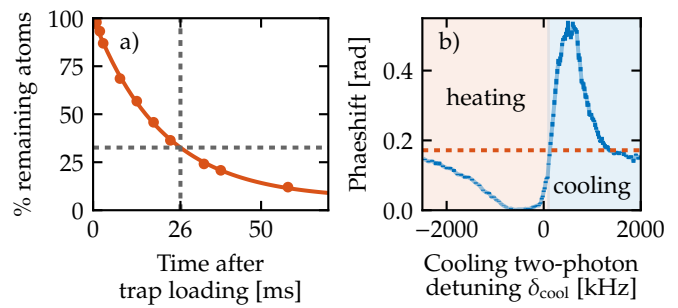


Figure 4. a) Remaining fraction of atoms in the trap without cooling as a function of time after trap loading. Solid line: Exponential fit. Dashed lines indicate the atomic signal after a waiting time of 26 ms. b) Atomic signal after 200 cooling cycles (duration 26 ms), as a function of cooling two-photon detuning, δ_{cool} , (solid line, dark error bars) and atomic signal without cooling for equal time after trap loading (dashed line).

different Zeeman states become degenerate, which we will utilize for obtaining a simple repump scheme for cooling – see below. Further, we observe a significant broadening of the transfer spectrum without the magnetic bias field. The line is broadened from essentially interaction-time limited width, to ~ 1 MHz FWHM. At least part of this broadening can be attributed to spatially varying vector light shifts from the blue-detuned trap light [20, 21]. We note that the same broadening is also observed in microwave transfer spectra under the same conditions.

The ability to couple motional states opens the possibility to apply Raman cooling of our ensemble, ultimately to the motional ground state. Raman cooling to the ground state has been demonstrated in nanoscale optical tweezer traps [22, 23]. In nanofiber traps, a significantly increased background heating rate, as compared to free space optical traps, is observed. This competes with the Raman cooling process, and various mechanisms to explain this effect have been put forward [5, 21, 24]. Without cooling the atomic population is heated from the trap, leading to a measured trap lifetime of 21 ms, see Fig. 4a. Similar values have been reported for other nanofiber traps [4–6, 8].

We implement a Raman cooling scheme as follows: Our atoms are prepared in the $|F=4\rangle$ level, without a magnetic bias field. A 40 μ s Raman pulse transfers a fraction of the atoms to $|F=3\rangle$, with a concomitant decrease (increase) of the motional quantum number for positive (negative) two-photon detuning of the cooling light δ_{cool} . After the Raman transfer, we turn on the MOT repump laser resonant to the $|F=3\rangle \rightarrow |F'=4\rangle$ transition for 60 μ s, which pumps atoms back into $|F=4\rangle$ after on average 1.7 scattering events, significantly lower than the number of scattering events needed for preparation of a pure Zeeman state in the presence of a bias field. With 200 repetitions, the total cooling sequence lasts 26 ms, somewhat longer than the $1/e$ -lifetime of the atoms in the

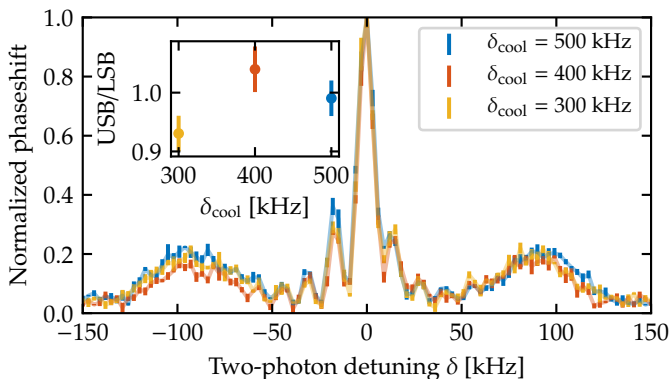


Figure 5. Raman transfer spectrum after 200 cooling pulses, for 3 different values of two photon detuning during cooling, δ_{cool} . The spectra are normalized for clarity, due to an overall difference in atoms in the trap after the cooling sequence. Inset: Ratio of the upper sideband (USB) to the lower sideband (LSB) integrated over the ranges $\pm(60 \text{ kHz} - 125 \text{ kHz})$, as a function of δ_{cool} . Error bars show 1σ statistical uncertainties.

trap. For cooling, the optical power of the Raman beam and pulse duration were optimized for maximum transfer efficiency on the sideband transition $|F=3\rangle \otimes |n\rangle \rightarrow |F=4\rangle \otimes |n+1\rangle$ in the presence of a magnetic bias field of 3 G.

To assess the effect of cooling, we turn on the probe and MOT repumper, and measure the remaining atoms, as shown in Fig. 4b as a function of δ_{cool} . For $\delta_{\text{cool}} \lesssim 0 \text{ kHz}$ we observe a clear reduction of the atomic signal, whereas for $100 \text{ kHz} \lesssim \delta_{\text{cool}} \lesssim 1 \text{ MHz}$ the signal increases by up to a factor of 3.1, compared to the case of no cooling.

To further analyze the cooling performance, we perform the same cooling sequence, after which we ramp up the bias field to 3 G and prepare the atoms in $|F=3, m_F=0\rangle$ by optical pumping and microwave transfers [25]. We then record sideband-resolved Raman spectra with an optical Raman laser power similar to the one used in Fig. 3a. Example spectra for three different values of δ_{cool} are displayed in Fig. 5. The spectra show that we cannot reliably detect a pronounced decrease in the radial temperature of the atoms, heralded by a clear asymmetry between the upper and lower motional sidebands. In the inset we show the integrated sideband ratios (including 1σ statistical error bars). We observe a slight indication of an increase in the ratio for $\delta \sim 400 \text{ kHz}$, but the average motional quantum number remains significantly above $\bar{n} = 1$.

Several effects are prone to reduce the efficiency of the cooling scheme. Working with a broadened Raman line at zero bias field hinders the selective excitation of motional sidebands. Secondly, while the preparation of atoms into a specific state in the $|F=3\rangle$ -manifold (e.g. $|F=3, m_F=0\rangle$) is necessary for the resolved sidebands spectroscopy of the cooled ensemble, it comes at

the price of extra scattering events and extra time spent in the trap after the cooling sequence, increasing the temperature. We anticipate that in an improved setup a cooling protocol on a stretched level, e.g. $|F=3, m_F=3\rangle \rightarrow |F=4, m_F=4\rangle$ in the presence of a bias field can be implemented. This scheme still allows for a simple and efficient repump method, while motional sidebands are fully resolved.

We have presented a Raman coupling scheme for optical manipulation of Cs atoms, that further cancels all quadratic ac-Stark shifts. We have demonstrated coherent transfers using this scheme, as well as the cancellation of the Stark shifts.

By utilizing the radial decay of the Raman laser light we have shown that we can effectively couple the radial motional states by optical manipulation. We have further demonstrated first steps towards experimental implementation of cooling of the radial degree of freedom. We show that we can extend the lifetime of atoms in the trap by application of 200 pulses of Raman cooling.

In summary, we have detailed an experimentally feasible way for obtaining optical manipulation of neutral atoms around nanofibers using exclusively guided light modes. Optical manipulation of atoms trapped in nanoscale optical systems offers exciting new possibilities such as position-dependent manipulation and adiabatic pulses on timescales faster than the motional frequencies.

Funding: ERC grant INTERFACE (grant no. ERC-2011-ADG 20110209). The authors would like to thank Signe B. Markussen for help with data acquisition.

-
- [1] J. D. Thompson, T. G. Tiecke, N. P. de Leon, J. Feist, A. V. Akimov, M. Gullans, A. S. Zibrov, V. Vuletić, and M. D. Lukin, “Coupling a single trapped atom to a nanoscale optical cavity,” *Science* **340**, 1202–1205 (2013).
 - [2] A. Goban, C.-L. Hung, S.-P. Yu, J. D. Hood, J. A. Muniz, J. H. Lee, M. J. Martin, A. C. McClung, K. S. Choi, D. E. Chang, O. Painter, and H. J. Kimble, “Atom-light interactions in photonic crystals,” *Nat. Commun.* **5**, 3808 (2014), arXiv:1312.3446 [physics.optics].
 - [3] D. O’Shea, C. Junge, J. Volz, and A. Rauschenbeutel, “Fiber-optical switch controlled by a single atom,” *Phys. Rev. Lett.* **111**, 193601 (2013), arXiv:1306.1357 [quant-ph].
 - [4] S. Kato and T. Aoki, “Strong coupling between a trapped single atom and an all-fiber cavity,” *Phys. Rev. Lett.* **115**, 093603 (2015), arXiv:1505.06774 [quant-ph].
 - [5] E. Vetsch, D. Reitz, G. Sagué, and A. Rauschenbeutel, “Optical interface created by laser-cooled atoms trapped in the evanescent field surrounding an optical nanofiber,” *Phys. Rev. Lett.* **104**, 203603+ (2010), arXiv:0912.1179 [quant-ph].
 - [6] A. Goban, K. S. Choi, D. J. Alton, D. Ding, C. Lacroûte, M. Pototschnig, T. Thiele, N. P. Stern, and H. J. Kimble, “Demonstration of a state-insensitive, compensated

- nanofiber trap,” *Phys. Rev. Lett.* **109**, 033603 (2012), 1203.5108.
- [7] J.-B. Béguin, E. M. Bookjans, S. L. Christensen, H. L. Sørensen, J. H. Müller, E. S. Polzik, and J. Appel, “Generation and detection of a sub-Poissonian atom number distribution in a one-dimensional optical lattice,” *Phys. Rev. Lett.* **113**, 263603 (2014), arXiv:1408.1266.
- [8] J. Lee, J. A. Grover, J. E. Hoffman, L. A. Orozco, and S. L. Rolston, “Inhomogeneous broadening of optical transitions of ^{87}Rb atoms in an optical nanofiber trap,” *J. Phys. B: At. Mol. Opt. Phys.* **48**, 165004 (2015), arXiv:1412.6754 [physics.atom-ph].
- [9] N. V. Corzo, B. Gouraud, A. Chandra, A. Goban, A. S. Sheremet, D. V. Kupriyanov, and J. Laurat, “Large Bragg reflection from one-dimensional chains of trapped atoms near a nanoscale waveguide,” *Phys. Rev. Lett.* **117**, 133603 (2016), arXiv:1604.03129 [quant-ph].
- [10] D. Hunger, T. Steinmetz, Y. Colombe, C. Deutsch, T. W. Hänsch, and J. Reichel, “A fiber Fabry-Perot cavity with high finesse,” *New. J. Phys.* **12**, 065038 (2010), arXiv:1005.0067 [physics.optics].
- [11] F. Haas, J. Volz, R. Gehr, J. Reichel, and J. Estève, “Entangled states of more than 40 atoms in an optical fiber cavity,” *Science* **344**, 180–183 (2014).
- [12] Pablo Solano, Jeffrey A Grover, Jonathan E Hoffman, Sylvain Ravets, Fredrik K Fatemi, Luis A Orozco, and Steven L Rolston, “Optical nanofibers: a new platform for quantum optics,” *Adv. Atom. Mol. Opt. Phys.* **66**, 439–505 (2017), 1703.10533.
- [13] B. Albrecht, Y. Meng, C. Clausen, A. Dareaux, P. Schneeweiss, and Arno Rauschenbeutel, “Fictitious magnetic-field gradients in optical microtraps as an experimental tool for interrogating and manipulating cold atoms,” *Phys. Rev. A* **94**, 061401 (2016), 1608.02517.
- [14] Mark Kasevich and Steven Chu, “Laser cooling below a photon recoil with three-level atoms,” *Phys. Rev. Lett.* **69**, 1741–1744 (1992).
- [15] J. Appel, A. MacRae, and A. I. Lvovsky, “A versatile digital GHz phase lock for external cavity diode lasers,” *Meas. Sci. Technol.* **20**, 055302+ (2009), arXiv:0809.3607 [quant-ph].
- [16] A. Louchet-Chauvet, J. Appel, J. J. Renema, D. Oblak, N. Kjærgaard, and E. S. Polzik, “Entanglement-assisted atomic clock beyond the projection noise limit,” *New. J. Phys.* **12**, 065032+ (2010), arXiv:0912.3895 [quant-ph].
- [17] The absolute cancellation point for atoms in $|F = 4, m_F = 0\rangle$ and $|F = 4, m_F = \pm 4\rangle$ is almost identical, as verified by explicit numerical calculations.
- [18] C. Østfeldt, *Coherent Optical Control and Cooling of Nanofiber-trapped Atoms*, Master’s thesis, University of Copenhagen (2017).
- [19] David J Wineland, C Monroe, Wayne M Itano, Dietrich Leibfried, Brian E King, and Dawn M Meekhof, “Experimental issues in coherent quantum-state manipulation of trapped atomic ions,” *J. Res. Natl. Inst. Stan.* **103**, 259 (1998).
- [20] D. Reitz, C. Sayrin, R. Mitsch, P. Schneeweiss, and A. Rauschenbeutel, “Coherence properties of nanofiber-trapped cesium atoms,” *Phys. Rev. Lett.* **110**, 243603 (2013), arXiv:1302.4792 [quant-ph].
- [21] C. Lacroûte, K. S. Choi, A. Goban, D. J. Alton, D. Ding, N. P. Stern, and H. J. Kimble, “A state-insensitive, compensated nanofiber trap,” *New Journal Of Physics* **14**, 023056 (2012), arXiv:1110.5372 [quant-ph].
- [22] A. M. Kaufman, B. J. Lester, and C. A. Regal, “Cooling a single atom in an optical tweezer to its quantum ground state,” *Phys. Rev. X* **2**, 041014 (2012).
- [23] J. D. Thompson, T. G. Tiecke, A. S. Zibrov, V. Vuletić, and M. D. Lukin, “Coherence and raman sideband cooling of a single atom in an optical tweezer,” *Phys. Rev. Lett.* **110**, 133001 (2013).
- [24] C. Wuttke, G. D. Cole, and A. Rauschenbeutel, “Optically active mechanical modes of tapered optical fibers,” *Phys. Rev. A* **88**, 061801 (2013), arXiv:1311.0916 [physics.optics].
- [25] P. Tremblay and C. Jacques, “Optical pumping with two finite linewidth lasers,” *Phys. Rev. A* **41**, 4989–4999 (1990).